

Comprehensive Analysis of Suspending Force for Improved Bearingless Switched Reluctance Motor with Permanent Magnets in Stator Yoke

Fangxu Li, Huijun Wang, Fengge Zhang and He Zhang
(Invited)

Abstract—Different from conventional switched reluctance motor(SRM), bearingless SRM not only provides torque but also supplies levitation force for free-friction of rotor. In order to make sure that bearingless SRM can steadily levitates in static and dynamic rotating operation, it is necessary to analyze suspending force. Therefore, suspending force performance of an improved bearingless SRM with permanent magnets in stator yoke is comprehensively investigated in this paper. Basic structure and operation principle with permanent magnets in stator yoke are introduced firstly. Furthermore, mathematical model is built up for design of suspending force. In addition, parametric analysis for levitation performance is implemented. Finally, validity of proposed method is verified by experimental results.

Index Terms—Analysis, bearingless, switched reluctance, suspending force.

I. INTRODUCTION

SWITCHED reluctance motor (SRM) has an excellent performance under special environments, because of inherent fault tolerance, robustness, tolerance of high temperature or in intense temperature variations[1-3]. In the meanwhile, magnetic bearing has some advantages such as no friction, no lubrication and long life, which is suitable for the high speed application. Combining advantages of SRM and magnetic bearing, the bearingless SRM is proposed. Compared with conventional separated magnetic levitation motor, bearingless SRM highly integrates motor and magnetic bearing [4]. It means motor not only supplies rotating torque but also provides levitation force. Therefore, they are particularly suitable to operate in special environments such as more

electric aircraft application [5].

Recently, several structures of bearingless SRM have been proposed. A radial force and torque control scheme was proposed for bearingless control of a 12/8 pole SRM which has auxiliary windings for radial force in stator poles [6]. The auxiliary winding produces radial force for rotor levitation between stator and rotor poles. At the same time, one hybrid rotor structure, called Morrison rotor, was introduced [7]. The rotor is a hybrid structure which includes a circular lamination stack for improving levitation performance and a multi-pole lamination stack of conventional rotor. Additionally, 8/6 type bearingless SRM with single winding was proposed [8]. In this method, three windings are loaded with different currents in each commutating period and three torques and three lateral forces can be generated. According to the published papers, one common problem in these existing structures is that there is strong coupling between torque and radial force. This is not good for the high speed control.

In order to reduce coupling from motor structure, hybrid stator poles concept structure has been proposed such as 8/10 and 12/12 [9-11]. In this structure, torque pole on the stator generates torque while radial force pole generates suspending force. However, when these two types of stator poles are working at the same time, the magnetic crossing between fluxes by these two poles is still difficult to be avoided in 8/10. In 12/12 structure, the motor consists of two single phase motor. Biased flux is provided by axial permanent magnet, which is installed between two motor in axial direction. However, axial permanent magnet occupies axial space, which results into that axial length has to be increased and critical speed decreases. In addition, power density is low due to single phase motor.

Therefore, in this paper, an improved bearingless SRM with permanent magnets in stator yoke is proposed to reduce axial space and produce higher torque based on 12/12 structure [12]. In order to investigate suspending force performance of proposed structure, basic operating principle for proposed structure and mathematical model for suspending force are described. In the meanwhile, effect of structure parameters on the levitation performance is also investigated. Finally, one prototype motor is designed and manufactured. The validity of proposed structure is verified by the experimental results.

II. IMPROVED BEARINGLESS SRM STRUCTURE

Manuscript was submitted for review on 26, September, 2018.

This work was supported by the National Natural Science Foundation of China under Grant 51777004.

Fangxu Li is with the Instrumentation Science and Opto-electronics Engineering, Beihang University(email: lifangxu318@163.com)

Huijun Wang is currently working in School of Instrumentation Science and Opto-electronics Engineering, Beihang University(email: huijun024@gmail.com)

Fengge Zhang is with the School of Electrical Engineering, Shenyang University of Technology. (email: zhangfg@sut.edu.cn)

He Zhang is currently a Senior Research Fellow and Director of the Best Motion Machine Drive Technology Centre, Power Electronics, Machines, and Control Research Group, the University of Nottingham (email: he.Zhang@nottingham.ac.uk)

Digital Object Identifier 10.30941/CESTEMS.2018.00044

This section investigates improved bearingless SRM based on 12/12 permanent magnet biased structure. The structure is introduced as an alternative to the 12/12 bearingless SRM, which reduce axial length and increase critical speed. In the meanwhile, two-phase motor is employed to improve torque performance.

Fig.1 shows 12/12 permanent magnet biased bearingless SRM. It can be found that each motor has 12/12 structure. The permanent magnet between two motors provides biased flux for generating suspending force. Therefore, axial permanent magnet occupies axial space, which causes that axial length has to be increased and critical speed decreases. In addition, torque density is low due to single phase motor.

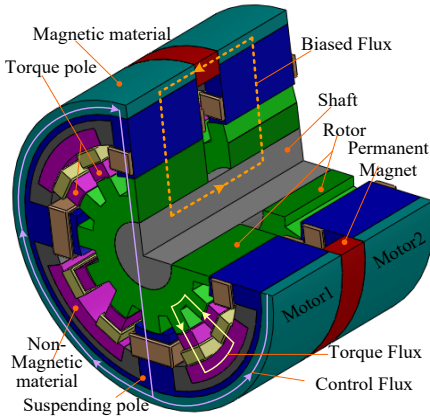


Fig.1. 12/12 permanent magnet biased bearingless SRM.

Fig.2 shows improved two-phase 12/14 structure. It can be found that four permanent magnets distribute uniformly in the stator yoke. In order to provide biased flux for suspending force, magnetizing of each permanent magnet is in circumferential direction. Same as 12/12 structure, there are two kinds of stator poles. One is called torque pole such as A1, A2. The other is called suspending pole such as T1, T2. There is magnetic isolation between torque and levitation pole using aluminum shield.

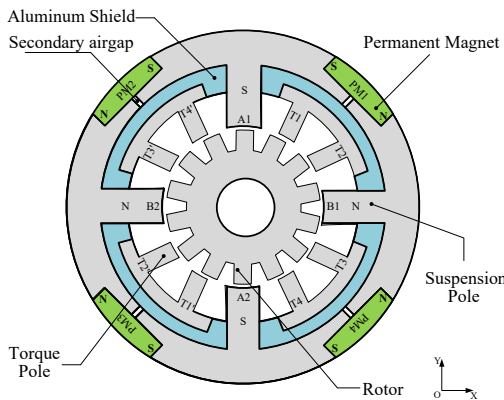


Fig.2. Improved 12/14 bearingless SRM with PMs in Stator Yoke.

Fig.3 shows operation principle of improved bearingless SRM. As shown in Fig.3(a), permanent magnet provides biased flux for levitation. Windings on the opposite suspending force poles in the diameter direction are connected in series to provide control flux. By means of overlapping of two flux of two air gap located oppositely in the diameter direction, resultant flux in one air gap increases while the other part

decrease. Consequently, one resultant force will be generated due to the magnetic field difference in the diameter direction.

During generation of levitation force, torque can be provided at the same time, as shown in Fig.3(b). It can be found that windings on the opposite torque poles in the diameter direction are connected in series to form one phase. For example, torque windings T1, T2, T1' and T2' are connected in series to form one phase while windings T3, T4, T3' and T4' form another phase. Therefore, proposed motor has two-phase structure, which improves torque performance compared with 12/12 structure.

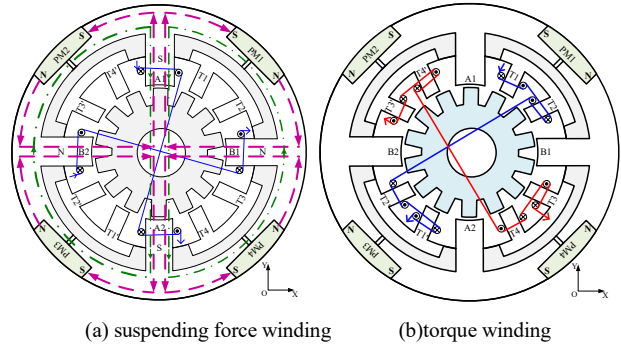


Fig.3. Operation principle of proposed bearingless SRM

III. SUSPENDING FORCE MODEL

As shown in Fig.3, the proposed motor has two different types of suspension magnetic flux. Equivalent magnetic circuits of PM bias flux and control flux at equilibrium position are shown in Fig. 4 and Fig. 5, respectively.

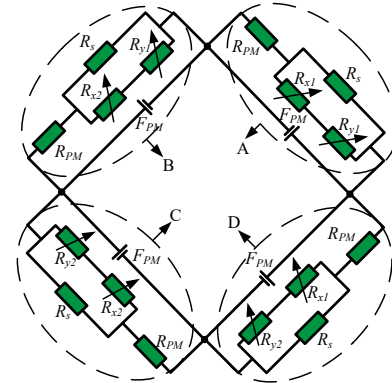


Fig.4. The equivalent magnetic circuit of the PM bias field.

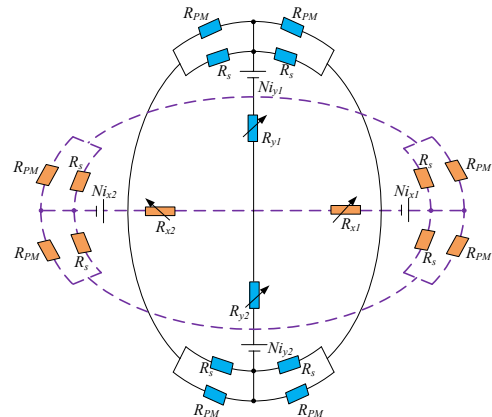


Fig. 5. Equivalent magnetic circuit of control flux.

In Fig. 4, R_s is the reluctance of the secondary air-gap, R_{x1} and R_{x2} are the reluctances of the suspension poles' air-gap with different direction in X channel, and R_{y1} and R_{y2} are the reluctances of the suspension poles' air-gap with different direction in Y channel. R_{PM} is the reluctances of each permanent magnet. In Fig.5, N is the turn number of winding coils. i_{x1} and i_{x2} are the control current in X channel's winding. i_{y1} and i_{y2} are the control current in Y channel's winding.

Considering symmetrical structure and independence, the each permanent magnet and the corresponding reluctances can be regarded as an independent part.

As for the bias flux produced by permanent magnet of each part, they can be defined as:

$$\begin{cases} \Phi_{x1pm} = \Phi_{PMA} \frac{R_{PMA} - R_{PM}}{R_{x1} + R_{y1}} + \Phi_{PMD} \frac{R_{PMD} - R_{PM}}{R_{x1} + R_{y2}} \\ \Phi_{x2pm} = \Phi_{PMB} \frac{R_{PMB} - R_{PM}}{R_{x2} + R_{y1}} + \Phi_{PMC} \frac{R_{PMC} - R_{PM}}{R_{x2} + R_{y2}} \\ \Phi_{y1pm} = \Phi_{PMA} \frac{R_{PMA} - R_{PM}}{R_{x1} + R_{y1}} + \Phi_{PMB} \frac{R_{PMB} - R_{PM}}{R_{x2} + R_{y1}} \\ \Phi_{y2pm} = \Phi_{PMC} \frac{R_{PMC} - R_{PM}}{R_{x2} + R_{y2}} + \Phi_{PMD} \frac{R_{PMD} - R_{PM}}{R_{x1} + R_{y2}} \end{cases} \quad (1)$$

where, Φ_{xipm} ($i=1,2$) is the flux at the air-gap in X direction provided by permanent magnet;

Φ_{yipm} ($i=1,2$) is the flux at the air-gap in Y direction provided by permanent magnet;

Φ_{PMi} ($i=A,B,C,D$) is flux of permanent magnet. It is defined as:

$$\begin{cases} F_{PM} = H_c I_{pm} \\ \Phi_{PMA} = \Phi_{PMB} = \Phi_{PMC} = \Phi_{PMD} = \frac{F_{PM}}{\sigma R_{PMi}} \end{cases} \quad (2)$$

in which, H_c is the coercive force of the permanent magnet; σ is the leakage coefficient of permanent magnet magnetic circuit; R_{PMi} ($i=A,B,C,D$) is the total reluctance of each part.

In order to simplify analysis, equivalent reluctance of each part in PM bias flux field is defined as:

$$\begin{cases} R_{PMA} = R_{PM} + \frac{1}{\frac{1}{R_s} + \frac{1}{R_{x1} + R_{y1}}} \\ R_{PMB} = R_{PM} + \frac{1}{\frac{1}{R_s} + \frac{1}{R_{x2} + R_{y1}}} \\ R_{PMC} = R_{PM} + \frac{1}{\frac{1}{R_s} + \frac{1}{R_{x2} + R_{y2}}} \\ R_{PMD} = R_{PM} + \frac{1}{\frac{1}{R_s} + \frac{1}{R_{x1} + R_{y2}}} \end{cases} \quad (3)$$

where, R_{PMi} ($i=A, B, C, D$) is the corresponding part's total reluctance; R_{PM} is the reluctance of the permanent magnet, it is defined as:

$$R_{PM} = \frac{l_{pm}}{\mu_0 \mu_r l_{da} h_{pm}} \quad (4)$$

where,

l_{pm} is the permanent magnet length in its magnetized direction;

l_{da} is the axial length of the stator core;

h_{pm} is the height of the permanent magnet;

$\mu_0 = 4\pi \times 10^{-7} H/m$ is the permeability in vacuum;

μ_r is the relative permeability of the permanent magnet.

And the reluctance of the secondary air-gap R_s is defined as:

$$R_s = \frac{\delta_s}{\mu_0 h_s l_{da}} \quad (5)$$

where

δ_s is the length of the secondary air-gap;

h_s is the height of the secondary air-gap.

Reluctances of air-gap A1, A2, B1 and B2 can be expressed as:

$$\begin{cases} R_{x1} = \frac{(y_{ror} + \delta_{x1})\delta_{x1}}{\mu_0 (2\delta_{x1}A_p - \delta_{x1}A_{ror} + A_p y_{ror})} \\ R_{x2} = \frac{(y_{ror} + \delta_{x2})\delta_{x2}}{\mu_0 (2\delta_{x2}A_p - \delta_{x2}A_{ror} + A_p y_{ror})} \\ R_{y1} = \frac{(y_{ror} + \delta_{y1})\delta_{y1}}{\mu_0 (2\delta_{y1}A_p - \delta_{y1}A_{ror} + A_p y_{ror})} \\ R_{y2} = \frac{(y_{ror} + \delta_{y2})\delta_{y2}}{\mu_0 (2\delta_{y2}A_p - \delta_{y2}A_{ror} + A_p y_{ror})} \end{cases} \quad (6)$$

in which, y_{ror} is the length of rotor's pole; A_p is the cross sectional area of stator pole; A_{ror} is the the cross sectional area of rotor pole; δ_{x1} , δ_{x2} , δ_{y1} and δ_{y2} are the length of suspension poles' air-gap in X and Y channel with different directions, respectively.

Similarly, when current flows through the control windings, control flux will produce, which flows through each air-gap can be defined as following:

$$\begin{cases} \Phi_{x1em} = \Phi_{x2em} = \frac{F_{ix}}{R_x \sigma_a} \\ \Phi_{y1em} = \Phi_{y2em} = \frac{F_{iy}}{R_y \sigma_a} \end{cases} \quad (7)$$

$$\begin{cases} \Phi_{sem} = \frac{\Phi_{y1em} (R_y - R_{y1} - R_{y2})}{2R_s} \\ \Phi_{pmem} = \frac{\Phi_{y1em} (R_y - R_{y1} - R_{y2})}{2R_{pm}} \end{cases} \quad (8)$$

where, Φ_{xiem} ($i=1,2$) is the flux at the air-gap in X direction provided by winding coils; Φ_{yiem} ($i=1,2$) is the flux at the air-gap in Y direction provided by winding coils; σ_a is the leakage coefficient of electromagnetic magnetic circuit.

And the magnetomotive force provided by control winding coils is depended on the turns of winding coils N and the current flowing through the control winding coils. As the control winding's connection type is in series, the current values and

the numbers of turns twinned on A1&A2 or B1&B2 are the same. The magnetomotive force can be calculated as:

$$F_{ix} = 2Ni_x \quad (9)$$

$$F_{iy} = 2Ni_y \quad (10)$$

in which, F_{ix} is the magnetomotive force provided by winding coils in X channel; F_{iy} is the magnetomotive force provided by winding coils in Y channel. And i_x is the control current in X channel's winding coils; i_y is the control current in Y channel's winding coils.

Total reluctance of control winding in each channel can be expressed as:

$$R_x = R_{x1} + R_{x2} + R_{pq} \quad (11)$$

$$R_y = R_{y1} + R_{y2} + R_{pq} \quad (12)$$

in which, R_{pq} is the parallel reluctance of permanent magnet and the secondary air-gap. R_{pq} can be expressed as:

$$R_{pq} = \frac{1}{\frac{1}{R_{PM}} + \frac{1}{R_s}} \quad (13)$$

To produce the suspension force, the fluxes produced by PM and control windings will add up. The total flux in each air-gap of suspension pole is expressed as:

$$\begin{cases} \phi_{x1} = \Phi_{x1pm} - \frac{F_{ix}}{R_x \sigma_a} \\ \phi_{x2} = \Phi_{x2pm} + \frac{F_{ix}}{R_x \sigma_a} \\ \phi_{y1} = \Phi_{y1pm} - \frac{F_{iy}}{R_y \sigma_a} \\ \phi_{y2} = \Phi_{y2pm} + \frac{F_{iy}}{R_y \sigma_a} \end{cases} \quad (14)$$

where, the Φ_{x1} , Φ_{x2} , Φ_{y1} and Φ_{y2} are the flux of the suspension pole A1, A2, B1 and B2.

As the magnetic force is related to the flux, the suspension force F_x and F_y in X and Y channel can be defined as:

$$F_x = \frac{180(\phi_{x1}^2 - \phi_{x2}^2)\delta}{\mu_0 \beta_r \pi R_{ror} l_{da}} \quad (15)$$

$$F_y = \frac{180(\phi_{y1}^2 - \phi_{y2}^2)\delta}{\mu_0 \beta_r \pi R_{ror} l_{da}} \quad (16)$$

in which, θ ($^\circ$) is the pole arc of rotor pole, R_{ror} is the outer radius of rotor.

By means of Taylor and neglecting higher order component, suspending force in (15) and (16) can be expressed as follows:

$$F = + \quad (17)$$

where, $k_x = (\partial F / \partial x)|_{x=0}$ is defined as displacement stiffness, $k_i = (\partial F / \partial i)|_{i=0}$ is defined as current stiffness.

IV. EFFECT OF PARAMETERS ON LEVITATION FORCE

Based on above model, suspending force is related on motor

parameters such as permanent magnet and air-gap. Fig.6 and Fig.7 show effect of permanent magnet parameters on levitation force performance.

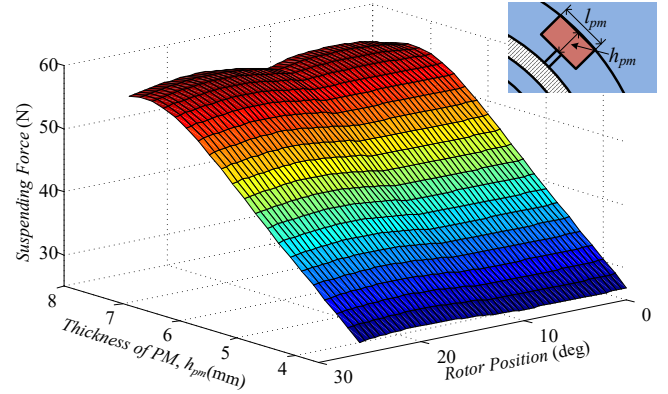


Fig.6. Effect of PM thickness on suspending force.

As shown in Fig.6, it can be found that with increasing of thickness from 3.6mm to 7.6mm, suspending force almost increases from 26.7N to 56.18N. Due to increasing of thickness, flux by permanent magnet rises. According to (14)-(15), suspending force is in direct proportion to square of flux. Consequently, force can be raised.

Fig.7 shows influence of permanent magnet thickness on current stiffness and displacement stiffness.

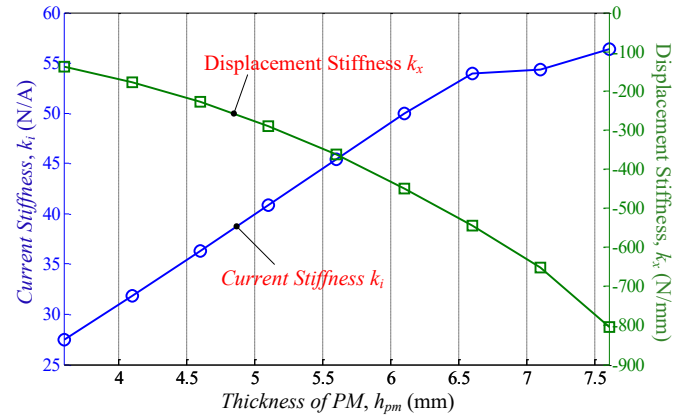


Fig.7. Effect of PM thickness on stiffness.

From Fig.7, it can be seen that when thickness rises to 6.6mm, current and displacement stiffness proportionally increase. However, when thickness is bigger than 6.6mm, flux density is higher, which causes saturation in stator yoke. Accordingly, increasing ratio of current stiffness is reduced. In addition, when thickness changes from 3.6mm to 7.6mm, current stiffness increases from 27.5N/A to 56.35N/A. For displacement stiffness, it varies from -138.5N/mm to -803.9N/mm. And value of displacement stiffness is negative. From the viewpoint of suspending force control, higher current stiffness is good for steady suspension.

Fig.8 shows variation in length of air-gap δ with respect to suspending force. It can be seen that suspending force is inversely proportional to the length of air-gap. When δ changes from 0.25mm to 0.5mm, average suspending force decreases

from 89.5N to 38.6N. As a result, a conclusion can be drawn that a smaller air-gap is hoped to get a larger suspending force.

Fig.9 shows effect of air-gap length on current stiffness and displacement stiffness. According to Fig.9, it can be seen that with variation of length of air-gap, current and displacement stiffness changes nonlinearly. when length of air-gap changes from 0.2mm to 0.5mm, current stiffness is reduced from 82N/A to 28.23N/A, where variation ratio is approximately three times. While displacement stiffness changes from -110.8N/mm to -188.33N/mm, in which variation ratio is approximately six times. Based on above analysis, length of air-gap is very sensitive to two kinds of stiffness.

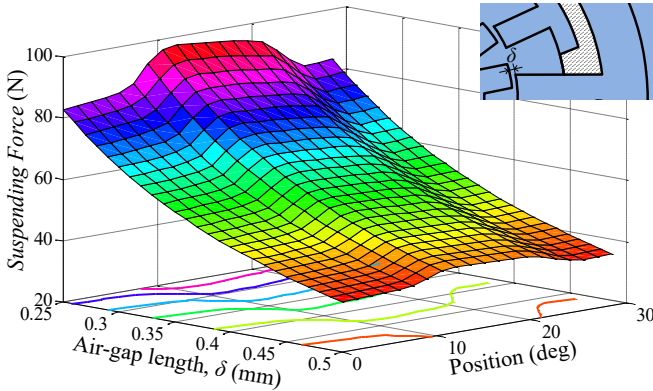


Fig.8. Effect of air-gap length δ on suspending force.

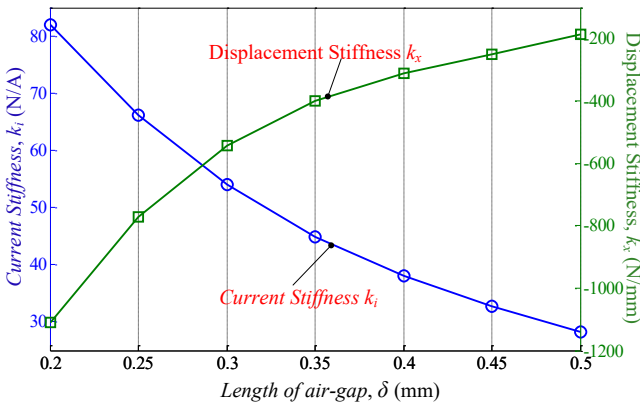


Fig.9. Effect of air-gap length on stiffness.

Fig.10 shows variation suspending force with respect to length of secondary air-gap δ_s. It can be seen that suspending force increases in direct proportion to length of secondary air-gap. When length increases from 0.4mm to 1.2mm, average suspending force increases from 47.51N to 54.74N. However, when length reaches to 0.6mm, increasing ratio gradually decreases. The reason is that leakage flux of permanent magnet nonlinearly decreases with increasing of secondary air-gap length.

Fig.11 shows effect of secondary air-gap length on current stiffness and displacement stiffness. When length of secondary air-gap increase from 0.4mm to 1.2mm, current stiffness rises from 47.52N/A to 54.74N/A while displacement stiffness changes from -470.49N/mm to -608.92N/mm.

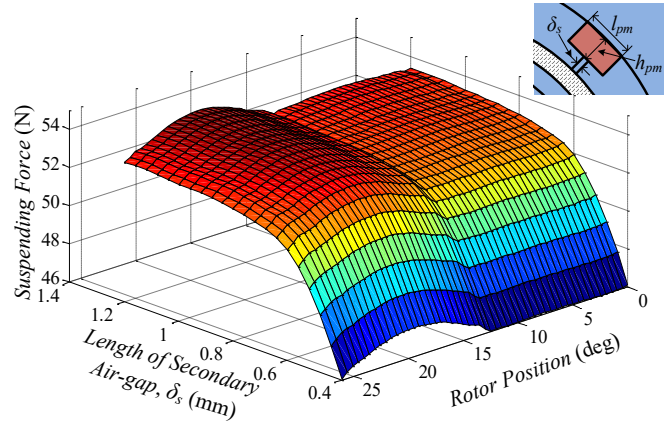


Fig.10. Effect of secondary air-gap length δ_s on suspending force.

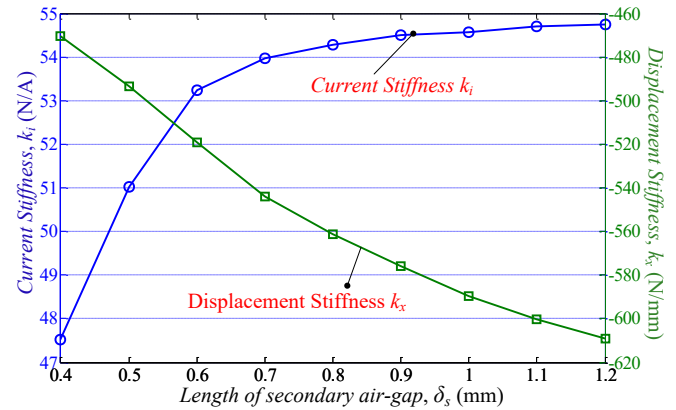


Fig.11. Effect of secondary air-gap length δ_s on stiffness.

V. PROTOTYPE MOTOR AND EXPERIMENTS

In order to verify above analysis method, one prototype motor is manufactured as shown in Table I. Fig.12 shows experimental platform. When balance weight is applied to shaft by means of load device, rotor will be eccentric from center position. And then, in order to make rotor move to center position, current of control winding should be controlled. Through applying different balance weights, relation between suspending force and current is attained.

TABLE.I THE SPECIFICATIONS OF PROPOSED MOTOR

Parameter	Value
Outside diameter of suspending pole	132mm
Inside diameter of suspending pole	56.6mm
Outside diameter of torque pole	108mm
Inside diameter of torque pole	56.6mm
Arc angel of suspending pole teeth	25deg
Arc angel of torque pole teeth	12deg
Outside diameter of rotor pole	56mm
Inside diameter of rotor pole	20mm
Rotor yoke height	9mm
Arc angel of rotor pole teeth	13deg
Permanent magnet width	10mm
Permanent magnet height	6.6mm
Main air-gap length	0.3mm
Secondary air-gap length	0.7mm
Number of control winding turns	80
Number of torque winding turns	120
Axial length of stator core	45mm

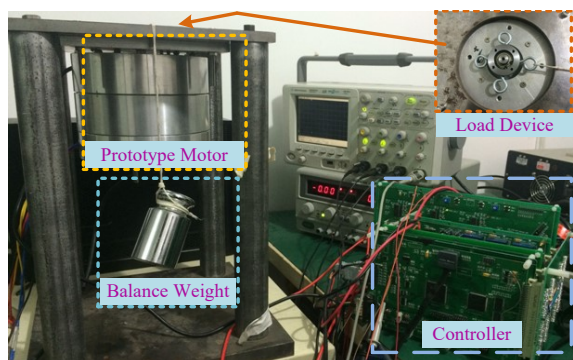


Fig.12. Experimental platform.

According to (17), compared current and displacement stiffness results between mathematic model and experiment are shown in Table II. It can be found that current stiffness error is 3.06% and displacement stiffness error is 6.81%, which can verify validity of mathematic model of suspending force.

TABLE.II Compared results of current and displacement stiffness

	Current stiffness	Displacement stiffness
Mathematic model	53.16 N/A	-609.24 N/mm
Experimental value	51.58 N/A	-570.38 N/mm
Error	3.06%	6.81%

Fig.13 shows rotor eccentric displacements and currents of two degrees of freedom, respectively, in static condition. Motor speed command is set to be zero. Displacement given commands of two suspending channels are set to be zero for keeping the rotor position in the center. It can be seen that the rotor moves to its balanced position after controller was applied under the static condition. In order to investigate effect of torque load variation on suspending performance, speed step experiment is implemented. Fig.14 shows the rotor eccentric displacement with speed step from 1000rpm to 5000rpm. It can be found that rotor can be kept the balanced position in the rotating condition. Fig.15 shows motor performance when radial force load variation happens. It can be found that rotor also can be controlled in balanced position while speed and torque current are almost constant.

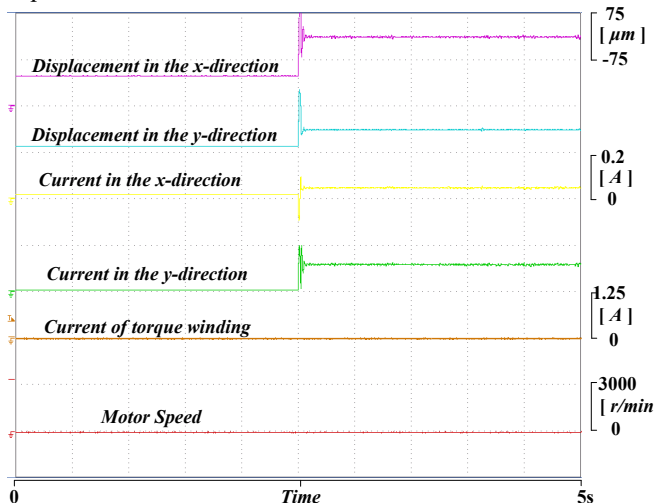


Fig.13. Rotor eccentric displacement and current under static condition.

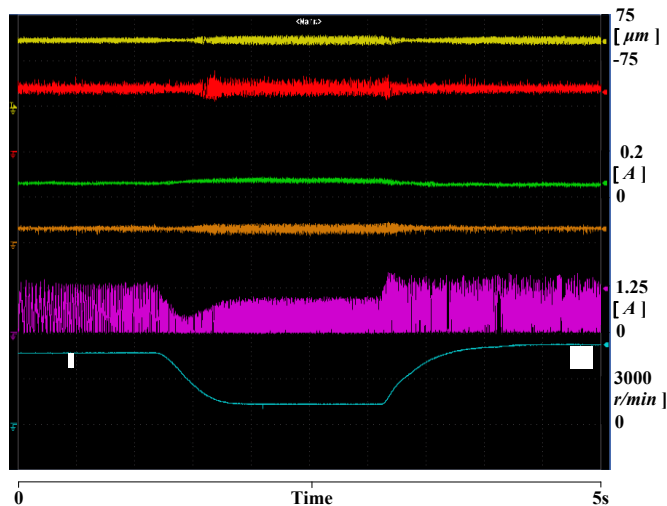


Fig.14. Speed step results under dynamic condition.

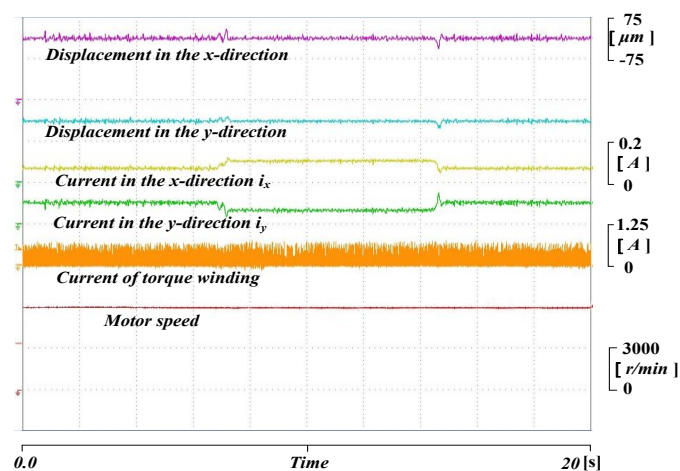


Fig.15. Radial force load step results under dynamic condition.

VI. CONCLUSION

In this paper, suspending force of a bearingless SRM with permanent magnets in stator yoke is comprehensively analyzed. Effect of different parameters on suspending force is investigated based on mathematic model. With increasing of permanent magnet thickness, suspending force is also increasing. However, suspending force results is exactly opposite for length of air-gap. In the meanwhile, variation trend of current and displacement stiffness with different parameters is similar to that of suspending force. From experimental results, mathematic model value of force is a close to testing value and error is small. Additionally, steady and dynamic operation is realized to verify validity of analysis method for suspending force.

REFERENCES

- [1] Jianning Dong, James Weisheng Jiang and etc, "Hybrid Acoustic Noise Analysis Approach of Conventional and Mutually Coupled Switched Reluctance Motors," *IEEE Transactions on Energy Conversion*, vol.32, no.3, pp.1042-1051, 2017

- [2] Wen Ding, Yanfang Hu, Tao Wang and Shuai Yang, "Comprehensive Research of Modular E-Core Stator Hybrid-Flux Switched Reluctance Motors With Segmented and Nonsegmented Rotors," *IEEE Transactions on Energy Conversion*, vol.32, no.1, pp.382-393, 2017
- [3] Teng Guo, Nigel Schofield and Ali Emadi, "Double Segmented Rotor Switched Reluctance Machine With Shared Stator Back-Iron for Magnetic Flux Passage," *IEEE Transactions on Energy Conversion*, vol.31, no.4, pp.1278-1286, 2016
- [4] M. Takemoto, A. Chiba, H. Akagi, and T. Fukao, "Radial force and torque of a bearingless switched reluctance motor operating in a region of magnetic saturation," *IEEE Trans. Ind. Appl.*, vol.40, no.1, pp.103-112, Jan./Feb. 2004
- [5] X. Cao, Z. Deng, G. Yang, and X. Wang, "Independent control of average torque and radial force in bearingless switched-reluctance motors with hybrid excitations," *IEEE Trans. Power Electron.*, vol.24, no.5, pp.1376-1385, May. 2009
- [6] Yan Yang, Zhiqian Deng, Gang Yang, Xin Cao, Qianying Zhang, "A Control Strategy for Bearingless Switched-Reluctance Motors," *IEEE Trans. Power Electron.*, vol.25, no.11, pp.2807-2819, 2010
- [7] Carlos R. Morrison. Bearingless Switched Reluctance Motor. U.S. Patent 6,727,618, 2004
- [8] Li Chen, W. Hofmann, "Speed Regulation Technique of One Bearingless 8/6 Switched Reluctance Motor With Simpler Single Winding Structure," *IEEE Trans. Ind. Electron.*, vol.59, no.6, pp.2592-2600, Jun. 2012
- [9] H.J. Wang, Y.Y. Wang, X.Q. Liu and J.W. Ahn, "Design of novel bearingless switched reluctance motor," *IET Electric Power Applications*, vol.6, no.2, pp.73-81, 2012
- [10] H.J. Wang, J.F. Liu, J.F. Bao and B.K. Xue, "A Novel Bearingless Switched Reluctance Motor with Biased Permanent Magnet," *IEEE Trans. Ind. Electron.*, vol.61, no.12, pp.6947-6955, 2014
- [11] H.J. Wang, J.F. Bao, B.K. Xue and J.F. Liu, "Control of Suspending Force in Novel Permanent-Magnet-Biased Bearingless Switched Reluctance Motor," *IEEE Trans. Ind. Electron.*, vol.62, no.7, pp.4298-4306, 2015
- [12] Bingkun Xue, Huijun Wang, Junfang Bao, "Design of novel 12/14 bearingless permanent magnet biased switched reluctance motor," Proceedings of 17th International Conference of Electrical Machines and Systems. Hangzhou, 2014: 2655-2660



Fangxu Li received the B.S. degree from China University of Mining & Technology, Beijing, China, in 2017. He is studying for M.S. degree in Instrumentation Science and Opto-electronics Engineering, Beihang University, Beijing, China. His research interest includes motor design and motor control.



Huijun Wang received the M.S. degree in electrical engineering from Shenyang University of Technology, Shenyang, China, in 2003 and Ph.D. degree in electrical and mechatronics engineering from Kyungsung University, Busan, Korea, in 2009. He is currently working in School of Instrumentation Science and Opto-electronics Engineering, Beihang University, Beijing, China. His research interest includes motor design and drive system.



Fengge Zhang was born in 1963. He received the B.E.E., M.S., and Ph.D. degrees from the Shenyang University of Technology, Shenyang, China, in 1990, and 2000, respectively, all in electrical engineering. Since 1984, he has been a Teacher with the School of Electrical Engineering, Shenyang University of Technology, where he is currently a Professor. He has been confirmed as the Young Academic Skeleton by Liaoning Province and the National Machinery Industry Ministry, respectively. From October 2001 to July 2002, he was a Visiting Scholar with the Esslingen University of Applied Sciences, Esslingen am Neckar, Germany. His research and teaching interests include electric-magnetic theory, dynamic simulation, magnetic-field analysis, optimized design, computer control technology of electrical machines, and wind power generating systems. He is also active in the area of power converters for variable-speed control and drive systems.



He Zhang received the B.Eng. degree in automatic control from Zhejiang University, Hangzhou, China, in 2002, and the Ph.D. degree in electrical machines from The University of Nottingham, Nottingham, U.K., in 2009. He then joined the U.K. Water Research Centre, Wiltshire, U.K., and worked on energy efficiency determination for motor drive systems for two years. He is currently a Senior Research Fellow and Director of the Best Motion Machine Drive Technology Centre, Power Electronics, Machines, and Control Research Group, the University of Nottingham. His research interests include high-performance electric machines and drives.